Physics of Fluids

RESEARCH ARTICLE | SEPTEMBER 25 2024

Compound cavity formation and splash crown suppression by water entry through proximally adjacent polystyrene beads

Daren A. Watson; Sebastian Anzola; Freddy A. Zeas; Korrie B. Smith; Anthony A. Cruz

Physics of Fluids 36, 092124 (2024)
https://doi.org/10.1063/5.0226769

Physics of Fluids ARTICLE pubs.aip.org/aip/pof

Compound cavity formation and splash crown suppression by water entry through proximally adjacent polystyrene beads

Cite as: Phys. Fluids **36**, 092124 (2024); doi: 10.1063/5.0226769
Submitted: 3 July 2024 · Accepted: 25 August 2024 ·
Published Online: 25 September 2024

View Online Export Citation CrossMark

Daren A. Watson,[a] Sebastian Anzola, Freddy A. Zeas, Korrie B. Smith, and Anthony A. Cruz

AFFILIATIONS

Mechanical Engineering Department, Florida Polytechnic University, Lakeland, Florida 33805, USA

[a]Author to whom correspondence should be addressed: dwatson@floridapoly.edu

ABSTRACT

We move forward the important topic of water entry by documenting splash dynamics arising from the impact of hydrophilic spheres with buoyant millimetric microplastics, mimicked in our study by polystyrene beads. Collision with small, buoyant beads is yet another means to manipulate splash dynamics. In this experimental study, we investigate the fluid–structure interactions between beads and hydrophilic spheres for Froude numbers in the range of $20-100$. Generally, hydrophilic spheres entering a liquid bath below the critical velocity of 8 m/s produce minimal fluid displacement and no cavity formation. The presence of proximally adjacent beads atop the fluid with respect to impacting spheres promote flow separation and compound cavities for sufficiently large Froude numbers, while suppressing the growth of splash crowns. Compound cavities consist of a shallow, quasi-static first cavity that seals near the water line, and a second, deeper cavity produced in the wake of descending spheres. A vertically protruding Worthington jet follows cavity collapse. The resulting splash metrics differ from those of hydrophobic spheres with respect to the properties of impacted beads. We find impactors traversing a deep liquid pool layered with beads experience drag reduction when compared to entry into a clean pool due to the drag-reducing benefits of flow separation while not offering a high inertial penalty. Our study unravels the physics behind the widely encountered interaction of solid projectiles impacting passively floating particles, and our results translate to the entry dynamics of water-diving creatures and projectiles into water bodies polluted by floating millimetric microplastics.

I. INTRODUCTION

The water entry of spherical projectiles have garnered the attention of fluid dynamicists since the early work of Worthington[1–3] in the late 19th century and is traditionally investigated in the context of impactor shape,[4,5] surface roughness,[6–8] and impact velocity.[9] The established literature shows relevance to toilet dynamics,[10–12] missile water entry,[6,13–21] animal locomotion,[22–25] sea-surface landing,[26,27] and underwater transport.[8,10–12] To date, the vast majority of water entry studies have been performed with unaltered free surface conditions.[6] Notwithstanding, there exists a few studies that have explored water entry in the context of a barrier to entry atop a deep liquid pool by the inclusion of a bubble layer;[28] an oil layer;[29] penetrable fabrics;[10] and non-penetrable fabrics,[12] respectively. Speirs *et al.* showed the radius-dependent nature of cavity-producing velocity when spheres enter a water–surfactant mixture containing dish washing liquid.[28] The inclusion of a bubble layer atop the water–surfactant mixture however ensures cavity formation at all tested impact velocities. Smolka and McLaughlin explored the influence of inertia on the morphology of oil-induced cavities and found that spheres with low inertia form smooth cavities, while those with high inertia develop rough cavity walls due to shear-induced instabilities between the oil layer and surrounding water.[29] Watson *et al.* employed thin, penetrable, nonwoven fabrics atop a liquid bath and showed the production of quasi-static cavities at impact velocities well below the required cavity-producing velocity ~ 8 m/s for hydrophilic impactors.[10] Threshold velocity[9] U for cavity formation as a function of the sphere's advancing contact angle θ_a is shown in Fig. 1(a). Watson *et al.* probed further by employing thin, non-penetrable fabrics atop the free surface and observed fabric-dependent cavities and jets.[12] In the current study, we explore the water entry dynamics of hydrophilic spheres through a free surface layered with beads within the range of Froude number $\mathrm{Fr} = U^2/gD = 20-100$, where $U \approx (2gh)^{1/2}$ is the sphere impact velocity, $g = 9.81$ m/s^2 is the acceleration due to gravity, $h = 20-75$ cm are the sphere release heights, and $D = 1.6$ and 2.0 cm are the sphere diameters. We herein move beyond previous studies by modifying the free surface with a disaggregated, particulate barrier to entry, and by connecting bead properties to entry dynamics.

During water entry, hydrophilic spheres experience no flow separation or air-entrainment for impact velocities[9] below $U \approx 8$ m/s as shown in Fig. 1(b) (Multimedia view). In contrast, hydrophobic spheres impacting a deep liquid pool experience flow separation and cavity formation at entry speeds well below 8 m/s as shown in Fig. 1(c) (Multimedia view), with the velocity threshold a function of the impactors' hydrophobicity[12] according to the theoretical predictions of Duez *et al.*[9] [Fig. 1(a)]. The resulting splashes consist of radial splash crowns[30] and significantly higher Worthington jets compared to their hydrophilic counterparts. Splashes arising from hydrophobic impactors may be tuned by entry velocity,[9,31,32] impactor rotation,[16,33] impactor shape,[5,34] impactor wettability,[9] surface tension,[35–37] fluid–solid density ratio,[15,16] and fluid viscosity.[26,38,39] Here, we provide the first documented investigation on the interfacial interaction of free-falling hydrophilic spheres with floating beads, an example of which is shown in Fig. 1(d) (Multimedia view), with respect to the influence of bead diameter d, bead density ρ'', and bead packing density χ on splash crown heights λ, cavity depths κ, splash heights Γ, and hydrodynamic drag coefficients C_D. For some tests, we apply hydrophobic coating to the spheres to investigate the limits of splash metrics with respect to bead properties.

Beyond the confines of the experimental work, there exists a high propensity for the collision of spherical projectiles with floating debris due to the prevalence of pollution in marine environments.[40–42] Such environments are plagued with buoyant microplastics varying from 10 μm to 5 mm in length.[43] Moreover, we note the probable presence of similarly sized semi-aquatic insects, an example of which is the water strider[25] whose herding atop ponds and lakes may serve as a disaggregated barrier to water entry. Here, we systematically investigate splash behavior generated by impacting spheres with millimetric floating beads, accounting for bead sizes 50% below and above the upper range ~5 mm for microplastics often reported in marine environments. As such, our results provide new insight into the splash dynamics of projectiles and may translate to water-diving creatures interacting with tainted aqueous pools. We present our experimental methods for bead property measurements and water entry experiments in Sec. II. Results and theoretical considerations are presented in Sec. III, and the implications of this work discussed in Sec. IV. We conclude the study in Sec. V.

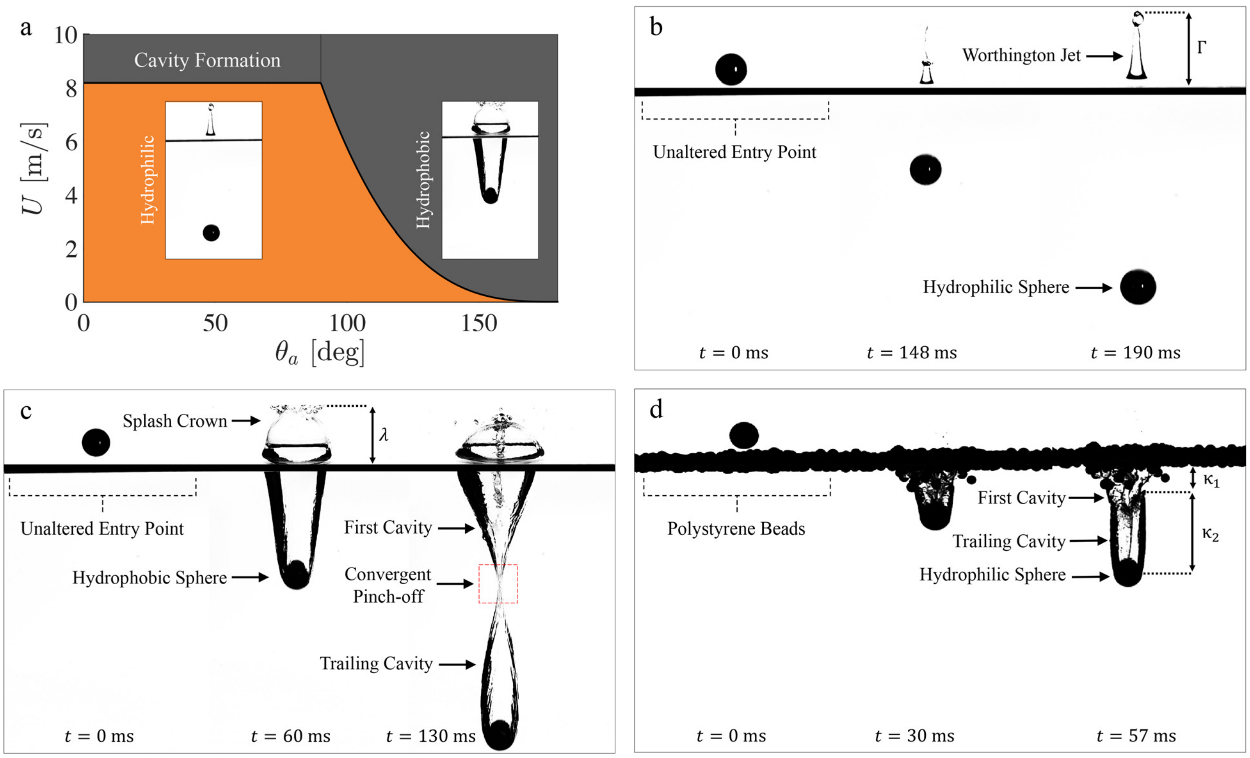

FIG. 1. (a) Threshold velocity U for cavity formation as a function of the advancing contact angle θ_a, based on theoretical predictions[9] of Duez *et al.* (b) Hydrophilic sphere entry through a quiescent free surface showing the absence of an air-entraining cavity, and the formation of a protruding Worthington jet. Jet heights are denoted by Γ and are measured at their maximum values. (c) Hydrophobic sphere entry through a quiescent free surface showing the presence of a prominent splash crown, and the formation of compound cavities in the wake of the descending sphere. Splash crown heights are denoted by λ and are measured at their maximum values. (d) Hydrophilic sphere entry through a free surface layered with beads showing the formation of compound cavities below the cavity-producing velocity for smooth impactors. Beads pictured have a diameter of $d = 5.08$ mm. Cavity depths are determined at the moment of seal between the first and trailing cavities.[8] The first cavity depth is denoted by κ_1, and the length of the trailing cavity by κ_2. Spheres pictured have diameter $D = 2.0$ cm, impact velocity $U = 3.13$ m/s, and Fr = 48. Multimedia available online.

II. METHODS

A. Bead property measurements

We employ three variations of polystyrene beads for surface alteration with diameters: 2.54 mm (bead A), 5.08 mm (bead B), and 7.62 mm (bead C). Dry ρ''_{dry} and wet ρ''_{wet} densities are measured by weighing individual balls on a digital analytical balance. To measure wet mass, we gently rest balls atop a small pool of water for 1 min to allow capillary motion to completely wet the material.[12] This method ensures that beads are not over-saturated before placement on the analytical balance. All measurements are replicated at least 15 times and the averages tabulated in Table I. We observe dry ρ''_{dry} and wet ρ''_{wet} densities are equal for beads on test in keeping with the hydrophobic nature of polystyrene.[44] The equilibrium contact angle of water on polystyrene beads is $\theta_{\mathrm{e}} = 109°$, measured photographically using a syringe to deposit water onto the beads' surface.[12] Despite varying packing densities χ, we keep surface packing uniform across all tests by ensuring individual beads rest side-by-side throughout the available free surface area $\sim$2700 cm^2. Thus, free-falling spheres collide with a single bead layer prior to water entry.

B. Water entry experiments

Smooth stainless steel spheres of masses $m = 16.6$ and 28.6 g and diameters $D = 1.6$ and 2.0 cm are released into a 122-L, 45-cm deep aquarium, filled halfway with tap water as shown in Fig. 2. Our choice of aquarium ensures negligible wall effects[19] from interaction with the tank given maximum sphere-to-tank diameter ratio $D/D_{\mathrm{tank}} \approx 0.04$, whereas $D/D_{\mathrm{tank}} > 0.05$ promotes the influence of wall effects. The equilibrium and advancing contact angles of water on hydrophilic impactors are $\theta_{\mathrm{e}} = 63°$ and $\theta_{\mathrm{a}} = 68°$, respectively, and are measured photographically using a syringe to deposit water onto the spheres' surface.[12] Impacting hydrophilic spheres are allowed to dry before each trial to preclude the influence of surface wetness. To conduct hydrophobic tests, we coat spheres with Rust-Oleum NeverWet. With the spray nozzle 30 cm away, spheres are sprayed twice with the base coat and allowed to dry for 30 min, before twice applying the top coat. Coated spheres are allowed to dry for at least 12 h before use in experiments. The equilibrium and contact angles of water on coated spheres are $\theta_{\mathrm{e}} = 105°$ and $\theta_{\mathrm{a}} = 128°$, respectively, measured photographically using a syringe to deposit water onto the spheres' surface.[12] Impacting hydrophobic spheres do not require cleaning, and are allowed to dry before each trial to preclude the influence of residual water on the spheres' surface.

Spheres are held above the target fluid using a custom-built, 3D-printed robotic arm, which facilitates rapid release from drop heights in the range $h = 20 - 75$ cm such that free fall is purely vertical and irrotational. Our switch-controlled robotic arm, which is powered by an Arduino Uno, is an enhanced approach from established water entry protocols that often rely on electromagnetism[6] or hand-held reclining levers.[11] Impact trials are replicated at least three times. Mean and standard deviation values are analyzed for measurements, and error bars included in plots where appropriate to show reproducibility of results. We film impacts with a Photron Mini AX-100 high-speed camera at 2000 frames per second using a 120-mm Nikon lens. We extract position track data and geometric measurements from videos using Open-Source Physics Tracker[12] and evaluate sphere kinematics with MATLAB®.

TABLE I. Measured material properties of polystyrene beads.

Polystyrene beads	d (mm)	ρ''_{dry} (mg/mm^3)	ρ''_{wet} (mg/mm^3)	χ (beads/cm^2)
Bead A	2.54	0.06	0.06	5.09
Bead B	5.08	0.06	0.06	1.27
Bead C	7.62	0.04	0.04	0.55

III. RESULTS

We impact passively floating beads atop the free surface of a deep aqueous pool with two smooth, free-falling hydrophilic spheres, coated hydrophobic for some tests, from various heights and compare changes in splash crown heights λ/D, cavity depths κ/D, jet heights Γ/D, and hydrodynamic drag coefficients C_{D} with respect to impacts on an unaltered, clean surface. Curve fitting correlation values for geometric measurements are tabulated in Table II. The inclusion of beads atop the free surface suppresses splash crown ascension and promotes flow separation below the velocity threshold required for non-cavity producing impactors while reducing hydrodynamic drag experienced by descending spheres.

A. Beads suppress splash crowns

Non-cavity forming splashes from spherical impactors typically include a thin, ascending film that travels along the surface of descending impactors as shown in Fig. 3(a), leading to the subsequent formation of a Worthington jet.[10] On the other hand, cavity-forming splashes from spherical impactors experience a well-developed arch above the water line whose rim contains miniature jets that form an axisymmetric film[10] as shown in Fig. 3(b). Hydrophilic spheres impacting proximally adjacent beads produce no splash crowns (no non-zero measurements) as shown in Fig. 3(c), notwithstanding the increased impact inertia illustrated in the qualitative comparison across varying Fr in Fig. 5. To further probe the limit of beads on splash crown suppression, we coat spheres hydrophobic and compare splash crown heights arising from impacts with a clean, quiescent free surface and impacts onto a surface layered with beads. We note that hydrophobic spheres generally produce larger splash crowns than their hydrophilic counterparts, with this contrast a function of the degree of hydrophobicity.[9] Means, standard deviations, and curve fitting values for non-dimensionalized splash crown heights λ/D with respect to Fr are tabulated in Table II. Results show a 28% decrease in mean non-dimensionalized splash crown heights for impacts onto the smallest beads (bead A), and a 71% decrease for impacts onto the largest beads (bead C) relative to splash crowns arising from clean water impacts. Thus, we see that larger beads with smaller surface packing densities χ further attenuates splash crown heights arising from hydrophobic impactors. An example of such attenuation is shown in Fig. 3(d).

Consider a cavity-forming sphere released from rest h above the water bath. In the limit of an inviscid fluid, the sphere's kinetic energy $E_{\mathrm{k,s}} = \rho_{\mathrm{s}} \forall_{\mathrm{s}} g h$ will be converted into potential energy of the splash crown $E_{\mathrm{p,sc}} = \rho \forall_{\mathrm{sc}} g \lambda$, where ρ_{s} and $\forall_{\mathrm{s}}$ are the density and volume of the sphere, respectively, and $\rho = 997$ kg/m^3, $\forall_{\mathrm{sc}}$, and λ are the density of water, volume of the splash crown, and height of the splash crown, respectively. Therefore, we may write $\rho \forall_{\mathrm{sc}} g \lambda \sim \rho_{\mathrm{s}} \forall_{\mathrm{s}} g h$. Experience[12] mandates the diameter of a disturbance in a compliant fluid surface,

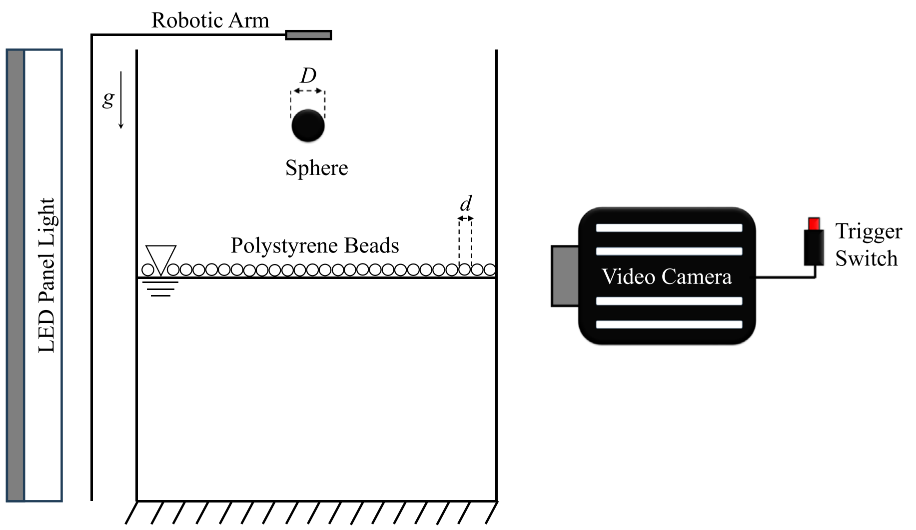

FIG. 2. Schematic of experimental setup. Photron Mini AX-100 camera captures frontal view of impacts with LED panel lights positioned behind the aquarium. Optional BNC trigger switch complements manual camera controls in video recording software. Switch-controlled robotic arm grips and releases spheres.

like water, is approximately equal to the diameter of the ensuing response, $\forall_s \sim \forall_{sc}$. Given ρ_s/ρ is a constant, we may write $\lambda \sim h$. To maintain non-dimensionality, $\lambda/D \sim h/D$. Noting that $\mathrm{Fr} = U^2/gD$, we obtain

$$\lambda/D \sim \mathrm{Fr} \tag{1}$$

for impacts atop the clean, quiescent free surface. Our *a priori* scaling result for splash crown heights coincides with the work of Cossali *et al.* who showed a strong dependence of crown heights on impact velocity.[30] We fit Eq. (1) to our experimental data in Fig. 4 and find the best fit correlation value $\mathrm{R}^2 = 0.79$ and best fit exponent $\alpha = 0.60$ for hydrophobic impactors according to $\lambda/D \sim \mathrm{Fr}^\alpha$. The deviation of α from unity may be attributed to experimental sensitivities as splash crown heights are quite variable in replicate tests for spherical impactors.[45] Accounting for the inclusion of beads atop the liquid bath during sphere collision, and thus, the added mass experienced during energy conversion with the coupled system $\rho + \rho''_{\mathrm{dry}}$, Eq. (1) becomes

$$\lambda/D \sim \varrho \mathrm{Fr}, \tag{2}$$

where $\varrho = \rho_s/(\rho + \rho''_{\mathrm{dry}})$. Thus, the presence of beads atop the water line dampens the resulting splash crown heights λ/D across the tested range of impact Fr. To mitigate the dampening effect of floating beads, free-falling spheres would require greater impact inertia by increasing Fr. Although $\rho''_{\mathrm{dry}} = \rho''_{\mathrm{wet}}$, given the hydrophobicity of polystyrene, we expect the integrity of Eq. (2) to maintain for more absorbent materials.

TABLE II. Mean, standard deviation, and curve fitting correlation values for splash crown heights λ/D, first cavity depths κ_1/D, trailing cavity depths κ_2/D, and jet heights Γ/D with respect to Froude number. Measurements corresponding to impacts with hydrophobic spheres are shown in boldface to create a distinction from impacts with hydrophilic spheres.

Measurements	Polystyrene beads	Mean	Standard deviation	Linear fit R^2	Best fit R^2
λ/D	Bead A	**0.81**	**0.18**	**0.18**	**0.81**
	Bead B	**0.37**	**0.15**	**0.85**	**0.85**
	Bead C	**0.33**	**0.14**	**0.56**	**0.59**
	Clean water	**1.12**	**0.31**	**0.52**	**0.79**
κ_1/D	Bead A	1.32	0.13	⋯	0.46
	Bead B	1.74	0.25	⋯	0.02
	Bead C	1.68	0.92	0.25	0.28
	Clean water	**3.66**	**0.99**	**0.74**	**0.93**
κ_2/D	Bead A	2.70	1.90	0.50	0.52
	Bead B	2.72	2.23	0.65	0.81
	Bead C	2.04	1.52	0.42	0.44
	Clean water	**5.32**	**0.89**	⋯	**0.95**
Γ/D	Bead A	3.81	1.89	0.79	0.81
	Bead B	2.68	1.55	0.73	0.77
	Bead C	2.30	1.52	0.61	0.67
	Clean water	3.11	0.74	0.32	0.83

B. Bead properties determine cavity dynamics

Hydrophilic spheres impacting proximally adjacent beads produce air-entraining cavities across all tested Fr as shown in Fig. 6. The presence of floating beads at the point of water entry promote flow separation well below the required cavity-forming velocity $U \sim 8$ m/s for smooth impactors.[9] In our study, the slowest cavity-producing velocity is approximately 2 m/s, which is equivalent to $U/4$. Prior to cavity seal,[6] we observe surface undulations in the cavity wall, such that we may describe a compound cavity consisting of two distinct regions, as shown in Fig. 5. This observation is analogous to cavity formation arising from clean water impacts with hydrophobic spheres. The cavity closest to the water line is a quasi-static[6,8] cavity characterized by contact with beads, which we denote as the "first cavity," with cavity depth κ_1. We note the bead-dependent nature of first cavities by the grouping of beads near the pinch-off location and posit that packing density χ is more determinate of non-dimensionalized first cavity depths κ_1/D as opposed to Froude number. First cavities are generally deeper for larger diameter beads, and in turn, smaller packing densities χ, which may be attributed to a higher resistance to water entry. Despite previously derived scaling arguments[8] showing $\kappa/D \sim \mathrm{Fr}$ for cavity-producing impactors, here $\mathrm{R}^2 = 0.74$, measurements in Fig. 6

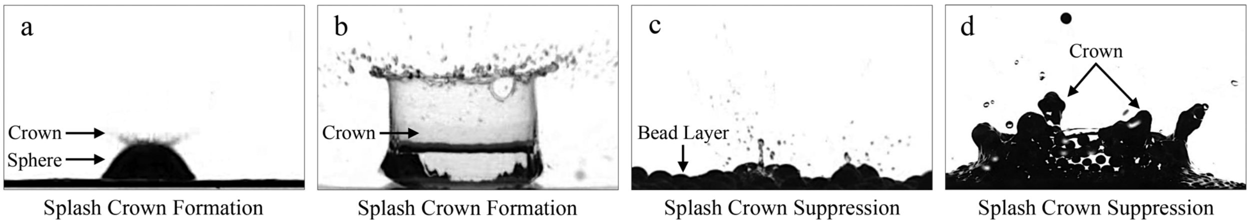

FIG. 3. Splash crown formation during the water entry of a (a) hydrophilic and (b) hydrophobic sphere for impacts onto a clean, quiescent liquid bath. Splash crown suppression during the water entry of a (c) hydrophilic and (d) hydrophobic sphere for the inclusion of beads atop the liquid bath. Beads pictured have a diameter of $d = 5.08$ mm. Impacting spheres have a diameter of $D = 2.0$ cm and impacts captured at $t = 30$ ms for Fr $= 54$.

reveal a weak correlation between non-dimensionalized first cavity depths κ_1/D and Fr. We note no linearity for measurements associated with bead A and bead B, and a near zero linearity ($R^2 = 0.25$) for measurements associated with bead C in Table II. Bead-dependent first cavities engulfing hydrophilic spheres are shallower than first cavities produced by hydrophobic spheres due to wall effects[19] resulting from the geometric confinement of cavities onset by contacting beads, as evidenced by measurements in Fig. 6. On average, bead-dependent cavity depths are 50% shallower than their hydrophobic counterparts as shown in Table II.

The second, deeper cavity region shown in Fig. 5 is smoother and vertically aligned behind the sphere, dubbed the "trailing cavity," with a cavity depth of κ_2. Compared to trailing cavities formed by hydrophobic spheres, bead-induced trailing cavities are more elongated with pinch-off diverging latitudinally across cavity walls [Fig. 5(b)], in contrast to pinch-off converging at a point for hydrophobic cavities [Fig. 1(c)]. The length of trailing cavities κ_2 are measured at the instant of first cavity seal.[12] Trailing cavities are uninhibited as opposed to first cavities, and remain attached to spheres until impact with the aquarium's floor. Like first cavities, trailing cavities are on average significantly shallower than their hydrophobic counterparts as shown in Table II. We fit $\kappa_2/D \sim \mathrm{Fr}$ to trailing cavity depths in Fig. 6 and obtain correlation values in the range $R^2 = 0.42 - 0.65$. Individual correlation values R^2 corresponding to each choice of beads on test are

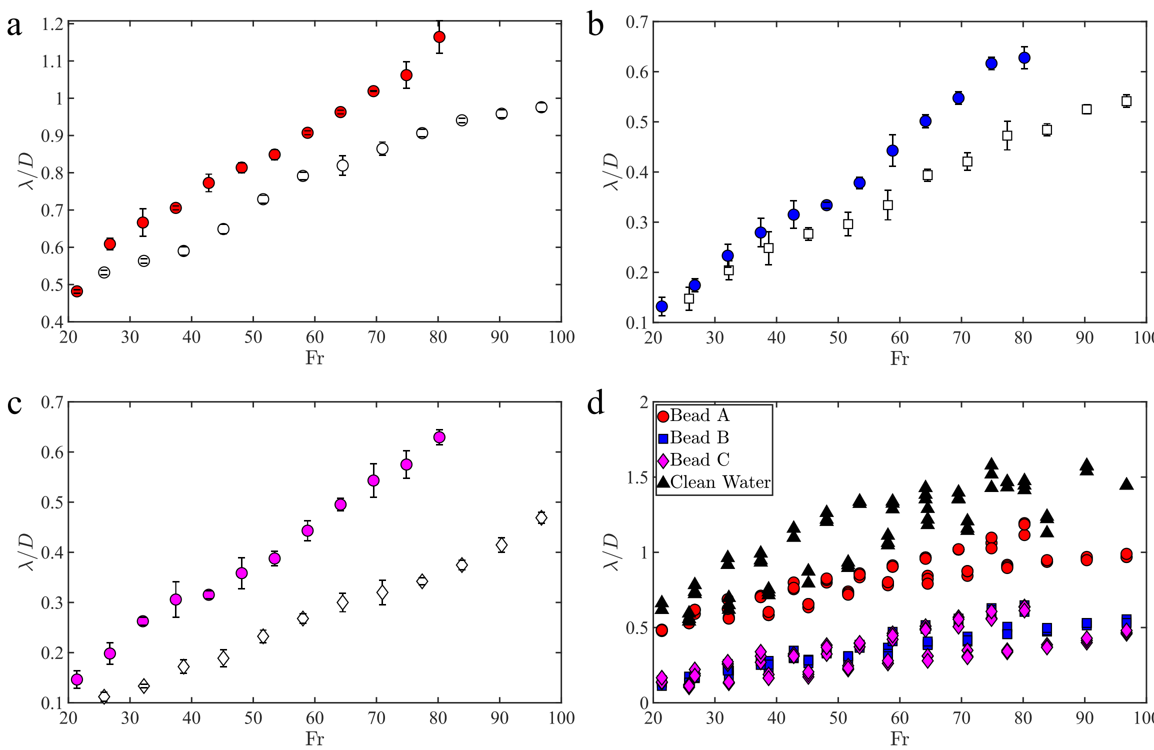

FIG. 4. Non-dimensionalized splash crown heights λ/D vs Froude number for hydrophobic sphere impacts onto a liquid bath layered with (a) bead A, (b) bead B, and (c) bead C. Bifurcation of data points in (a)–(c) is attributed to the different size spheres employed in the study. Unshaded symbols correspond to spheres with diameter $D = 1.6$ cm, while colored symbols correspond to spheres with diameter $D = 2.0$ cm. (d) Aggregated plot of non-dimensionalized splash crown heights λ/D vs Froude number for all tests. Linear and best fit predictions are analyzed, and correlation values tabulated in Table II.

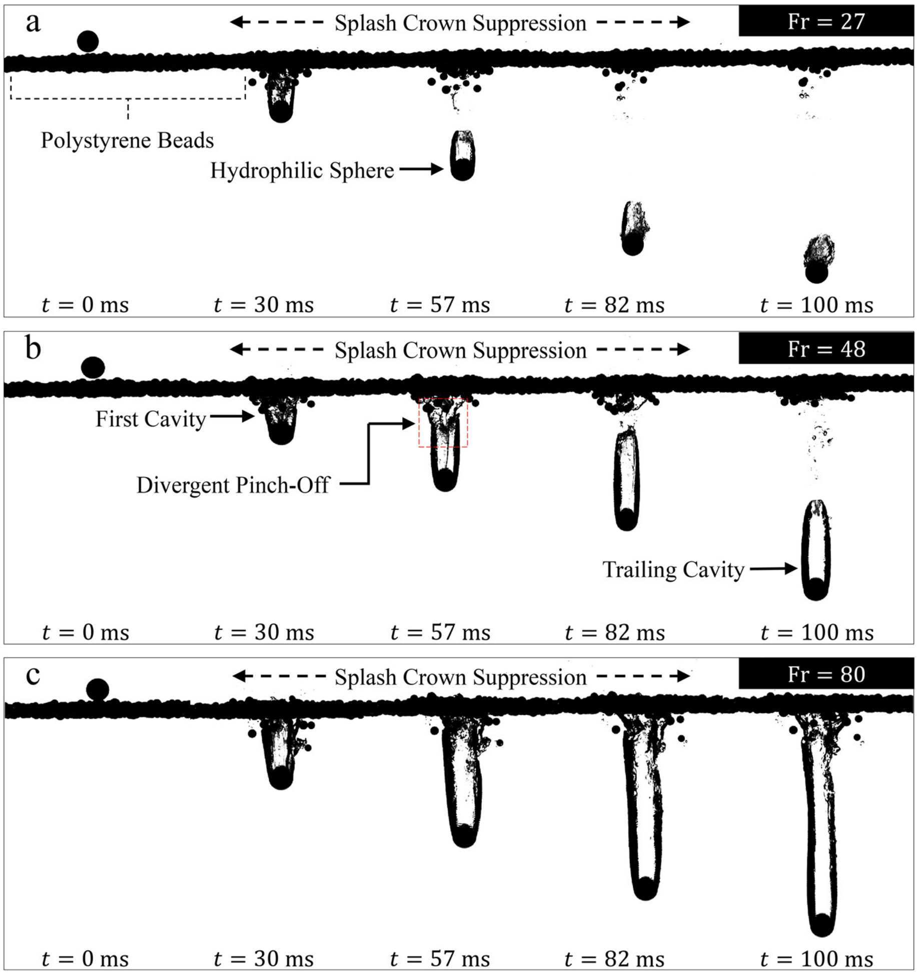

FIG. 5. Splash crown suppression and compound cavity formation for hydrophilic sphere impacts onto a liquid bath with interfacial entry point modified by a single layer of beads for (a) Fr = 27, (b) Fr = 48, and (c) Fr = 80. Beads pictured have a diameter of $d = 5.08$ mm. Spheres pictured have a diameter of $D = 2.0$ cm.

tabulated in Table II. Measurements show that $\kappa_2/D \to 0$ for some non-zero Fr, thereby revealing a critical Fr for trailing cavity formation. This observation is similar to the findings of Watson *et al.* who provided an additional fitting constant $c_1 < 0$ such that

$$\kappa_2/D = \phi \mathrm{Fr} + c_1, \tag{3}$$

where ϕ and c_1 are best fit coefficients.[8] Fitting Eq. (3) to measurements in Fig. 6 yield $\phi = 0.06$, $c_1 = -0.88$, $R^2 = 0.52$ for bead A, $\phi = 0.09$, $c_1 = -2.51$, $R^2 = 0.81$ for bead B, and $\phi = 0.05$, $c_1 = -0.59$, $R^2 = 0.44$ for bead C. Therefore, while the presence of beads promote flow separation and their size d and packing density χ influence the growth of first cavities, trailing cavities are only generated for increased impact Froude numbers beyond a threshold value. Here, the corresponding threshold Fr values for trailing cavity production are bead A: $\mathrm{Fr}^* = 43$, bead B: $\mathrm{Fr}^* = 54$, and bead C: $\mathrm{Fr}^* = 37$, respectively.

C. Trailing cavities promote higher Worthington jets

Worthington jets are formed above the free surface following the collapse of air-entraining cavities onset by the inclusion of floating beads as shown in Fig. 7(b). The perimeter of these jets are rugged in comparison to the smooth outline[6] typical for clean water impacts [Fig. 7(a)]. Jets also show the ability for bead transport given bead attachment to the ascending fluid structure. We measure jet heights Γ and show that the inclusion of proximally adjacent beads modulate heights with respect to an unaltered free surface. We plot non-dimensionalized jet heights Γ/D against Fr for all beads on test and observe higher jets for impacts with increased inertia as shown in Fig. 8. Our observations may be justified *a prior* by first considering the conversion of the sphere's kinetic energy $E_{k,s} = \rho_s \forall_s g h$ to potential energy of the jet $E_{p,s} = \rho \forall_j g \Gamma$, where $\forall_j$ is the volume of the jet. As such, $\rho \forall_j g \Gamma \sim \rho_s \forall_s g h$. Since ρ_s/ρ is constant, and $\forall_j \sim \forall_s$, we may write $\Gamma \sim h$. Again, noting that $\mathrm{Fr} = U^2/gD$, we obtain

$$\Gamma/D \sim \mathrm{Fr}. \tag{4}$$

The linear relationship predicted by Eq. (4) is verified by measurements in Fig. 8. Fitting Eq. (4) to measurements in Fig. 8 yield best fit correlation values in the range $R^2 = 0.61 - 0.79$ for all beads on test. Individual values are tabulated in Table II. Given minimal variation in non-dimensionalized first cavity depths κ_1/D with respect to Fr (Sec. III B), we posit that the collapse of trailing cavities is the primary

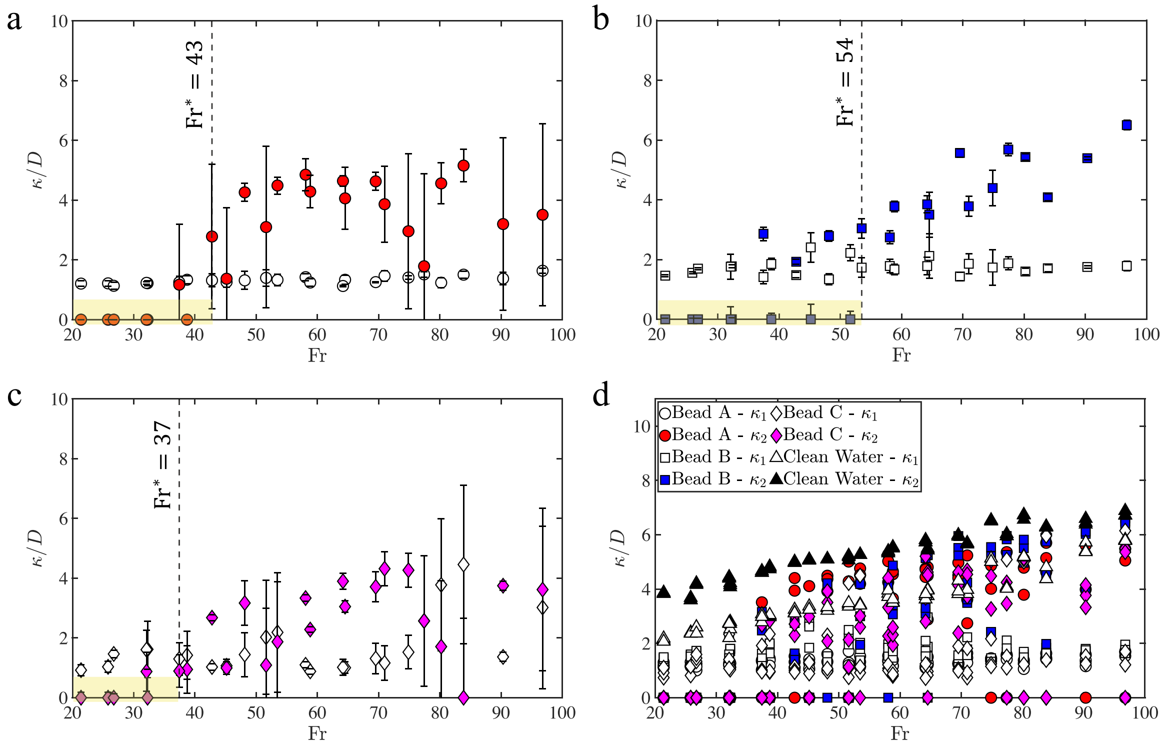

FIG. 6. Non-dimensionalized cavity depths κ/D vs Froude number for hydrophilic sphere impacts onto a liquid bath layered with (a) bead A, (b) bead B, and (c) bead C. (d) Aggregated plot of non-dimensionalized cavity depths κ/D vs Froude number for all tests. Unshaded symbols correspond to non-dimensionalized first cavity depths κ_1/D, while colored symbols correspond to non-dimensionalized trailing cavity depths κ_2/D. Trailing cavity measurements obtained below threshold Froude numbers (Fr^*) are highlighted in yellow on corresponding plots. Here, we note measurements labeled "Clean Water" correspond to cavities produced by hydrophobic spheres. Linear and best fit predictions are analyzed, and correlation values tabulated in Table II.

contributor to Worthington jet formation. In the limit of an inviscid fluid, as the trailing cavity retracts, the boundary work of the reclining cavity $W_{c,2} = \rho g D_{c,2}^2 \kappa_2^2$ is converted to gravitational potential energy in the jet $W_{j,1} = \rho g D_{j,1}^2 \Gamma^2$, where $D_{c,2}$ and D_j are the trailing cavity and jet diameters, respectively. Thus, we may write $\rho g D_{j,1}^2 \Gamma^2 \sim \rho g D_{c,2}^2 \kappa_2^2$. Similarly, experience mandates $D_j \sim D_{c,2}$. Accordingly, $\Gamma \sim \kappa_2$. To maintain non-dimensionality, $\Gamma/D \sim \kappa_2/D$. Substituting for Eq. (3), we may write

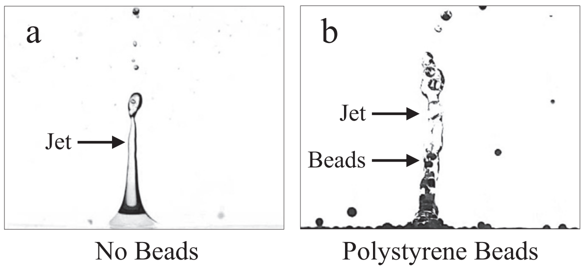

FIG. 7. Worthington jet formation during the water entry of a hydrophilic sphere for impacts onto a (a) clean, quiescent liquid bath and (b) a single bead layer. Beads pictured have a diameter of $d = 5.08$ mm. Impacting spheres have a diameter of $D = 2.0$ cm and impacts captured at $t = 150$ ms for Fr = 54.

$$\Gamma/D = \psi \mathrm{Fr} + c_2, \tag{5}$$

where ψ and c_2 are best fit coefficients.[8] Fitting Eq. (5) to measurements in Fig. 8 yield $\psi = 0.08$, $c_2 = -0.59$, and $R^2 = 0.81$ for bead A, $\psi = 0.06$, $c_2 = -0.87$, and $R^2 = 0.77$ for bead B, and $\psi = 0.06$, $c_2 = -0.89$, and $R^2 = 0.65$ for bead C, representing an improvement of correlation values previously obtained using Eq. (4). Therefore, we conclude that Worthington jets ascend higher for increased impact Fr beyond a critical value, akin to trailing cavity depths. Threshold Fr values (Fr^*) corresponding to trailing cavity depths are demarcated in Figs. 8(a) and 8(c).

D. Beads attenuate hydrodynamic drag

With respect to the water entry of spherical projectiles, it is well-established that hydrophobic spheres descend faster than their hydrophilic counterparts due to the dulling of vortex shedding.[18] To compare hydrodynamic forces induced by proximally adjacent beads, we fix $h = 50$ cm such that $U \approx 3.13$ m/s (Fr = 54) and track the center of mass of 2-cm spheres as seen in Fig. 9(a). Our chosen value of Fr ensures the presence of trailing cavities across impact trials, as reported in Sec. III B. Vertical position ($y-$ displacement) tracking is initialized when the center of mass of descending spheres transcend the water line ($y = 0$) and is discontinued just before impact with the aquarium's floor. Here, we do not quantify the role of hydrodynamic drag in the x

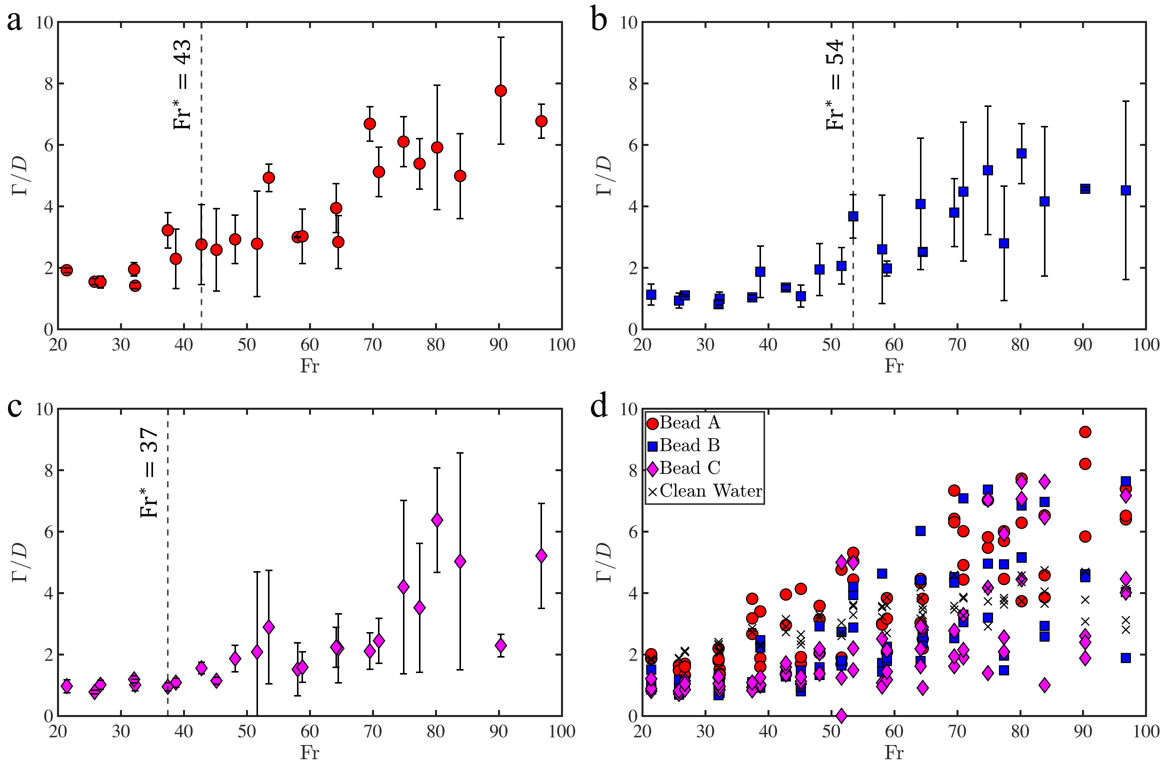

FIG. 8. Non-dimensionalized jet heights Γ/D vs Froude number for hydrophilic sphere impacts onto a liquid bath layered with (a) bead A, (b) bead B, and (c) bead C. (d) Aggregated plot of non-dimensionalized jet heights Γ/D vs Froude number for all tests. Linear and best fit predictions are analyzed, and correlation values tabulated in Table II.

direction since spheres experience no measurable lateral deviation[8,17,28] from straight-line trajectories at fluid entry. Considering Newton's second law of motion, a force balance for a sphere of mass m falling vertically into a quiescent liquid bath is given by[12]

$$F_D = mg - (m + m_a)a - F_B - F_\sigma, \tag{6}$$

where $F_D = \pi\rho U^2 C_D D^2/8$ is the hydrodynamic drag force acting on the sphere, a is the linear acceleration of the sphere, $m_a = \pi\rho D^3 C_m/6$ is the added mass, accounting for the effect of accelerating fluid by the descending sphere,[14] and $C_m = 0.5$ is the added mass coefficient, treated as constant across all cases.[14] While the value of C_m increases from zero at impact, the model presented here is not sensitive[12] to this change, given $m/m_a \sim O(10)$. Buoyancy force due to hydrostatic pressure is given by $F_B = \rho g(\pi D^3/6 + A(y)y)$, where y is the vertical position track, and $A(y)$ is the cross-sectional area of the sphere at the plane of flow separation.[12] For simplification, $A(y)$ is treated as constant by assuming separation at the equator such that $F_B = \rho g\pi(D^3/6 + D^2 y/4)$. For the range of Fr on test, we may neglect the force due to surface tension $F_\sigma = \sigma D$. As such, Eq. (6) can be rewritten as

$$du/dt = mg/m' - \rho g\pi D^2/8m'\left(4D/3 + 2y + C_D u^2/g\right), \tag{7}$$

where $m' = m + m_a$. We smooth vertical position track $y(t)$ with a Savitzky–Golay filter[12,46] to eliminate the effects of experimental error prior to numerical differentiation to obtain temporal velocity $u(t)$, and then smoothed again prior to a second and final numerical differentiation to obtain temporal acceleration $a(t)$.

Solving Eq. (7) numerically yields values of C_D in the range of instantaneous Reynolds number $\mathrm{Re} = \rho D u(t)/\mu = 54\,500 - 70\,000$, where $\mu = 8.90 \times 10^{-4}$ Pa s is the dynamic viscosity of water, as plotted in Fig. 9(b). To further compare drag coefficients C_D onset by beads, consider the following values for Re = 70 000: 0.29—bead A; 0.23—bead B; 0.67—bead C; 0.63—clean water; and 0.39—hydrophobic sphere. While our calculated value for hydrophobic spheres $C_D = 0.39$ is near the reference value reported in previous studies,[18] $C_D = 0.40$, the value for clean water impacts with hydrophilic spheres $C_D = 0.63$ deviates from the reference value[18] $C_D = 0.50$ (Re = 80 000) due to nuances arising from position tracking during sphere descent.[47] As previously reported in Watson *et al.*, numerous smoothing and differentiation techniques are available for analyzing position tracks,[12] such as that provided[47] by Epps *et al.* Such techniques are however less adaptable to experiments where the impacting sphere is shrouded by surface debris during water entry.[47] Thus, our employment of a Savitzky-Golay filter[8,10–12] and numerical differentiation may contribute to the deviation in clean water values for drag when compared to other studies. Notwithstanding, we observe that the inclusion of a bead layer atop the free surface reduces hydrodynamic drag experienced by descending hydrophilic spheres with respect to clean water impacts, with the limit of this reduction represented by bead C. These results can be viewed in the context of

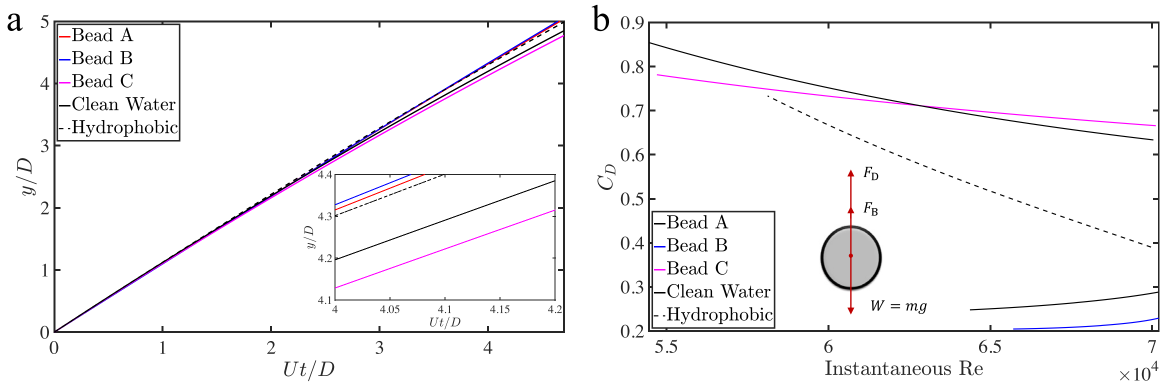

FIG. 9. (a) Non-dimensionalized vertical position *y*/*D* vs dimensionless time *Ut*/*D*. (b) Hydrodynamic drag coefficient C_D vs instantaneous Reynolds number Re.

Truscott *et al.*, who showed that non-cavity forming steel spheres with impacts in the range Re = 12 500 − 87 500 experienced higher drag than their cavity-producing counterparts due to pressure recovery and the initiation of vortex shedding in the wake of descending spheres.[18] We expect beads larger than bead C to provide greater inertial resistance at water entry such that spheres experience a net increase in drag despite the drag-reducing benefits of flow separation.

IV. DISCUSSION

In this study, we unveil the suppression of splash crowns; production of compound cavities; relation between trailing cavities and Worthington jets; and changes to hydrodynamic drag when hydrophilic spheres impact a liquid bath modified by the inclusion of proximally adjacent polystyrene beads. Beads provide increased resistance to water entry and restrict splash crown ascension for hydrophilic impactors. Likewise, splash crowns produced by hydrophobic impactors are significantly suppressed due to the added mass of the floating beads. Below the surface, bead-dependent first cavities are formed as spheres overcome the inertial requirements for water entry and experience minimal variation in depths with respect to changes in Froude number. First cavities are unable to produce uniform cavity walls typically observed for the water entry of hydrophobic spheres.[12] Instead, cavity walls appear jagged due to cavity interaction with beads and inherently result in pinch-off diverging across cavity walls, confirming the coupling of bead properties to cavity behavior. While our tests exhibit new pinch-off behavior for cavities, bead sizes beyond those tested may provide different patterns. Thus, the relation between bead properties and pinch-off dynamics is an area requiring further investigation.

Trailing cavities inspire the heights of Worthington jets. This observation corresponds to the results of Watson *et al.* who showed the onset of trailing cavities by punctured fabrics promoting higher Worthington jets.[12] The sphere's ability to pierce the modified free surface and the resulting cavity in its wake are paramount for ensuing jets. While we expect higher jets when spheres overcome greater resistance to water entry,[12] jets will become stymied at the limit of entry resistance due to the high inertial penalty experienced by spheres. As such, bead properties associated with the prohibition of Worthington jets require further probing as a means of tuning splashes.

When using beads to modulate splash features, it is important that spheres possess enough momentum with respect to bead properties to avail the drag-reducing benefits of flow separation. Our calculated drag coefficients $C_D \approx 0.23 - 0.67$ for hydrophilic sphere impacts with beads align with those for impacts onto fabrics $C_D \approx 0.27 - 0.68$ in the same Reynolds number range.[12] This result further reveals similarities between the employment of a disaggregated homogenous barrier like beads, and one that is intact like fabrics. For both, the inertial resistance offered at water entry incite compound cavities causing the suppression of trailing vortices[12] and the hastening of sphere descent with respect to clean water impacts. Going forward, a systematic investigation into the relation between non-solid surfactants and hydrodynamic drag is an avenue for new research.

Our study augmented the free surface of a deep liquid bath with a buoyant homogeneous bead layer using three choices of polystyrene beads. Given the interfacial contact of spheres and beads limited to the water line of the aquarium, beads exhibit influence most analogous to impactor wettability. Considering our cavity-inducing results with beads, and results previously determined by the deployment of a bubble layer,[28] an oil layer,[29] penetrable fabrics,[10] and non-penetrable fabrics,[12] we herein affirm another means by which the requirements for cavity formation by hydrophilic spheres can be reduced without altering the spheres' surface roughness. Additionally, while not tested, we note the thickness of the bead layer as another parameter for regulating splashes. Here, a single layer with thickness corresponding to bead diameter rests atop the free surface for impact trials. We believe that increasing bead layer thickness whether through bead size or stacking will further suppress splash crowns, attenuate cavities and jets, and slow spheres during water entry. The thickness at which splash features are eliminated is yet to be determined and provides an interesting area for future research.

For some cases, measurements corresponding to splash metrics have standard deviations of the same order of magnitude as the mean values, as shown in Table II. Despite replicating impact trials three times, which is typical for water entry studies,[8,12] such results reflect a strong degree of randomness attributed to the interfacial interaction of spheres with the floating bead layer. While beads are proximally adjacent, resting side-by-side, sensitivities onset by the interaction between individual beads within the bead layer and the oncoming sphere is still unknown. Further investigations beyond the range of our tested Froude numbers would unravel the influence of bead properties with respect to these experimental sensitivities. It is noteworthy to mention a similar challenge encountered by Watson *et al.*[10,12] where the randomness of fabric buckling during sphere impact was unavoidable, resulting in an unmitigable source of error. Thus, error mitigation for water entry experiments employing non-liquid surface modifiers is an important pursuit for future studies.

V. CONCLUSION

In contrast to water entry through a clean, quiescent free surface, splash crowns are restricted during hydrophilic sphere impacts, and significantly suppressed in the case of hydrophobic sphere impacts when the water bath is layered with floating, millimetric polystyrene beads. Here, hydrophilic spheres produce air-entraining cavities with textures and metrics dependent on bead properties and impact Froude number. Generally, increases in impact velocity promote the formation of trailing cavities attached to descending spheres until collision with the aquarium's floor. The depths of trailing cavities inspire the heights of Worthington jets vertically protruding above the liquid bath. The inclusion of beads atop the free surface hastens sphere descent despite resistance to water entry. Splash features may thus be tuned by bead properties.

ACKNOWLEDGMENTS

We would like to acknowledge the Florida Polytechnic University for partial support. We also thank David Vidana-Fuentes, Zamar Joseph, Gabriella Salas-Sivira, and Sabrina Roggero for experimental support.

AUTHOR DECLARATIONS

Conflict of Interest

The authors have no conflicts to disclose.

Author Contributions

Daren A. Watson: Conceptualization (lead); Data curation (lead); Formal analysis (lead); Funding acquisition (lead); Investigation (lead); Methodology (lead); Project administration (lead); Resources (lead); Software (lead); Supervision (lead); Validation (lead); Visualization (lead); Writing – original draft (lead); Writing – review & editing (lead). **Sebastian Anzola:** Data curation (supporting); Formal analysis (supporting); Investigation (supporting); Methodology (supporting); Validation (supporting); Visualization (supporting). **Freddy A. Zeas:** Data curation (supporting); Formal analysis (supporting); Investigation (supporting); Methodology (supporting); Validation (supporting); Visualization (supporting). **Korrie B. Smith:** Data curation (supporting); Formal analysis (supporting); Investigation (supporting); Methodology (supporting); Validation (supporting); Visualization (supporting); Writing – original draft (supporting). **Anthony A. Cruz:** Data curation (supporting); Formal analysis (supporting); Methodology (supporting); Visualization (supporting).

DATA AVAILABILITY

The data that support the findings of this study are available from the corresponding author upon reasonable request.

REFERENCES

[1]A. M. Worthington and R. S. Cole, "Impact with a liquid surface, studied by the aid of instantaneous photography," Philos. Trans. R. Soc. London, Ser. A **189**, 137–148 (1897).

[2]A. M. Worthington and R. S. Cole, "Impact with a liquid surface, studied by the aid of instantaneous photography, Paper II," Philos. Trans. R. Soc. London, Ser. A **65**, 153–154 (1900).

[3]A. M. Worthington, *A Study of Splashes* (Longmans, Green and Company, 1908).

[4]V. Duclaux, F. Caille, C. Duez, C. Ybert, L. Bocquet, and C. Clanet, "Dynamics of transient cavities," J. Fluid Mech. **591**, 1–19 (2007).

[5]Y. Kubota and O. Mochizuki, "Influence of head shape of solid body plunging into water on splash formation," J. Vis. **14**, 111–119 (2011).

[6]T. T. Truscott, B. P. Epps, and J. Belden, "Water entry of projectiles," Annu. Rev. Fluid Mech. **46**, 355–378 (2013).

[7]D. Li, J. Zhang, M. Zhang, B. Huang, X. Ma, and G. Wang, "Experimental study on water entry of spheres with different surface wettability," Ocean Eng. **187**, 106123 (2019).

[8]D. A. Watson, J. M. Bom, M. P. Weinberg, C. J. Souchik, and A. K. Dickerson, "Water entry dynamics of spheres with heterogeneous wetting properties," Phys. Rev. Fluids **6**, 044003 (2021).

[9]C. Duez, C. Ybert, C. Clanet, and L. Bocquet, "Making a splash with water repellency," Nat. Phys. **3**, 180–183 (2007).

[10]D. A. Watson, J. L. Stephen, and A. K. Dickerson, "Jet amplification and cavity formation induced by penetrable fabrics in hydrophilic sphere entry," Phys. Fluids **30**, 082109 (2018).

[11]D. A. Watson, J. L. Stephen, and A. K. Dickerson, "Impacts of free-falling spheres onto a deep liquid pool with altered fluid and impactor surface conditions," J. Vis. Exp. **144**, e59300 (2019).

[12]D. A. Watson, C. J. Souchik, M. P. Weinberg, J. M. Bom, and A. K. Dickerson, "Making a splash with fabrics in hydrophilic sphere entry," J. Fluids Struct. **94**, 102907 (2020).

[13]J. M. Aristoff, T. T. Truscott, A. H. Techet, and J. W. M. Bush, "The water entry cavity formed by low bond number impacts," Phys. Fluids **20**, 091111 (2008).

[14]J. Aristoff and J. Bush, "Water entry of small hydrophobic spheres," J. Fluid Mech. **619**, 45–78 (2009).

[15]J. Aristoff, T. Truscott, A. Techet, and J. Bush, "The water entry of decelerating spheres," Phys. Fluids **22**, 032102 (2010).

[16]T. Truscott and A. Techet, "Water entry of spinning spheres," J. Fluid Mech. **625**, 135–165 (2009).

[17]A. Techet and T. Truscott, "Water entry of spinning hydrophobic and hydrophilic spheres," J. Fluids Struct. **27**, 716 (2011).

[18]T. Truscott, B. Epps, and A. Techet, "Unsteady forces on spheres during free-surface water entry," J. Fluid Mech. **704**, 173–210 (2012).

[19]M. M. Mansoor, J. O. Marston, I. U. Vakarelski, and S. T. Thoroddsen, "Water entry without surface seal: Extended cavity formation," J. Fluid Mech. **743**, 295–326 (2014).

[20]D. Van Der Meer, "Wrapping up a century of splashes," J. Fluid Mech. **800**, 1–4 (2016).

[21]M.-H. Zhao, X.-P. Chen, and Q. Wang, "Wetting failure of hydrophilic surfaces promoted by surface roughness," Sci. Rep. **4**, 5376 (2014).

[22]D. L. Hu, B. Chan, and J. W. M. Bush, "The hydrodynamics of water strider locomotion," Nature **424**, 663–666 (2003).

[23]J. W. Bush and D. L. Hu, "Walking on water: Biolocomotion at the interface," Annu. Rev. Fluid Mech. **38**, 339–369 (2006).

[24]V. M. Ortega-Jimenez, L. von Rabenau, and R. Dudley, "Escape jumping by three age classes of water striders from smooth, wavy and bubbling water surfaces," J. Exp. Biol. **220**, 2809–2815 (2017).

[25]D. A. Watson, M. R. Thornton, H. A. Khan, R. C. Diamco, D. Yilmaz-Aydin, and A. K. Dickerson, "Water striders are impervious to raindrop collision forces and submerged by collapsing craters," Proc. Natl. Acad. Sci. U. S. A. **121**, e2315667121 (2024).

[26]A. May, "Effect of surface condition of a sphere on its water-entry cavity," J. Appl. Phys. **22**, 1219–1222 (1951).

[27]J. Shin and T. A. McMahon, "The tuning of a splash," Phys. Fluids A **2**, 1312–1317 (1990).

[28] N. Speirs, M. Mansoor, R. Hurd, S. Sharker, W. Robinson, B. Williams, and T. Truscott, "Entry of a sphere into a water-surfactant mixture and the effect of a bubble layer," Phys. Rev. Fluids **3**, 104004 (2018).
[29] L. B. Smolka and C. K. McLaughlin, "Sphere entry through an oil lens floating on water," Phys. Rev. Fluids **4**, 044001 (2019).
[30] G. E. Cossali, M. Marengo, A. Coghe, and S. Zhdanov, "The role of time in single drop splash on thin film," Exp. Fluids **36**, 888–900 (2004).
[31] J. Glasheen and T. McMahon, "Vertical water entry of disks at low Froude numbers," Phys. Fluids **8**, 2078–2083 (1996).
[32] S. T. Thoroddsen, T. G. Etoh, K. Takehara, and Y. Takano, "Impact jetting by a solid sphere," J. Fluid Mech. **499**, 139–148 (2004).
[33] T. T. Truscott, "Cavity dynamics of water entry for spheres and ballistic projectiles," Ph.D. thesis (Massachusetts Institute of Technology, 2009).
[34] N. Kim and H. Park, "Water entry of rounded cylindrical bodies with different aspect ratios and surface conditions," J. Fluid Mech. **863**, 757–788 (2019).
[35] E. Castillo-Orozco, A. Davanlou, P. K. Choudhury, and R. Kumar, "Droplet impact on deep liquid pools: Rayleigh jet to formation of secondary droplets," Phys. Rev. E **92**, 053022 (2015).
[36] Z. Che and O. K. Matar, "Impact of droplets on immiscible liquid films," Soft Matter **14**, 1540–1551 (2018).
[37] N. B. Speirs, Z. Pan, J. Belden, and T. T. Truscott, "The water entry of multi-droplet streams and jets," J. Fluid Mech. **844**, 1084–1111 (2018).
[38] J. Cheny and K. Walters, "Extravagant viscoelastic effects in the Worthington jet experiment," J. Non-Newtonian Fluid Mech. **67**, 125–135 (1996).
[39] A. Ogawa, K. Utsuno, M. Mutou, S. Kouzen, Y. Shimotake, and Y. Satou, "Morphological study of cavity and Worthington jet formations for Newtonian and non-Newtonian liquids," Part. Sci. Technol. **24**, 181–225 (2006).
[40] J. A. I. do Sul and M. F. Costa, "The present and future of microplastic pollution in the marine environment," Environ. Pollut. **185**, 352–364 (2014).
[41] J. G. Derraik, "The pollution of the marine environment by plastic debris: A review," Mar. Pollut. Bull. **44**, 842–852 (2002).
[42] G. G. N. Thushari and J. D. M. Senevirathna, "Plastic pollution in the marine environment," Heliyon **6**, e04709 (2020).
[43] A. Shamskhany, Z. Li, P. Patel, and S. Karimpour, "Evidence of microplastic size impact on mobility and transport in the marine environment: A review and synthesis of recent research," Front. Mar. Sci. **8**, 760649 (2021).
[44] K. Horie, I. Mita, J. Kawabata, S. Nakahama, A. Hirao, and N. Yamazaki, "Hydrophobicity and dynamic characteristics of cross-linked polystyrene gels studied with fluorescent probes," Polym. J. **12**, 319–328 (1980).
[45] M. Artman-Breitung, D. A. Watson, and A. K. Dickerson, "Simultaneous impact of twin drops on a semi-infinite liquid target," Phys. Fluids **33**, 102110 (2021).
[46] S. R. Krishnan and C. S. Seelamantula, "On the selection of optimum Savitzky-Golay filters," IEEE Trans. Signal Process. **61**, 380–391 (2013).
[47] B. P. Epps, T. T. Truscott, and A. H. Techet, "Evaluating derivatives of experimental data using smoothing splines," in Proceedings of Mathematical Methods in Engineering International Symposium (MMEI), Lisbon Portugal, 2010.